A&A 606, A77 (2017)
DOI: 10.1051/0004-6361/201731032

Astronomy & Astrophysics

Star formation in low density HI gas around the elliptical galaxy NGC 2865

F. Urrutia-Viscarra[1,2], S. Torres-Flores[1], C. Mendes de Oliveira[3], E. R. Carrasco[2], D. de Mello[4], and M. Arnaboldi[5,6]

[1] Departamento de Física y Astronomía, Universidad de La Serena, Av. Cisternas 1200 Norte, La Serena, Chile
e-mail: furrutia@userena.cl; furrutia@gemini.edu
[2] Gemini Observatory/AURA, Southern Operations Center, Casilla 603 La Serena, Chile
[3] Departamento de Astronomia, Instituto de Astronomia, Geofísica e Ciências Atmosféricas da USP, Rua do Matão 1226, Cidade Universitária, 05508-090 São Paulo, Brazil
[4] Observational Cosmology Laboratory, Code 665, Goddard Space Flight Center, Greenbelt, MD 20771, USA
[5] European Southern Observatory, Karl-Schwarzschild-Strasse 2, 85748 Garching, Germany
[6] INAF, Observatory of Pino Torinese, 10025 Turin, Italy

Received 24 April 2017 / Accepted 19 June 2017

ABSTRACT

Context. Interacting galaxies surrounded by HI tidal debris are ideal sites for the study of young clusters and tidal galaxy formation. The process that triggers star formation in the low-density environments outside galaxies is still an open question. New clusters and galaxies of tidal origin are expected to have high metallicities for their luminosities. Spectroscopy of such objects is, however, at the limit of what can be done with existing 8−10 m class telescopes, which has prevented statistical studies of these objects.
Aims. NGC 2865 is a UV-bright merging elliptical galaxy with shells and extended HI tails. In this work we aim to observe regions previously detected using multi-slit imaging spectroscopy.
Methods. We obtained new multi-slit spectroscopy of six young star-forming regions around NGC 2865, to determine their redshifts and metallicities.
Results. The six emission-line regions are located 16−40 kpc from NGC 2865 and they have similar redshifts. They have ages of ∼10 Myr and an average metallicity of $\sim 12 + \log(\mathrm{O/H}) \sim 8.6$, suggesting a tidal origin for the regions. We note that they coincide with an extended HI tail, which has projected density of $N_{\mathrm{HI}} < 10^{19}$ cm^{-2}, and displays a low surface brightness counterpart. These regions may represent the youngest of the three populations of star clusters already identified in NGC 2865.
Conclusions. The high, nearly-solar, oxygen abundances found for the six regions in the vicinity of NGC 2865 suggest that they were formed by pre-enriched material from the parent galaxy, from gas removed during the most recent major merger. Given the mass and the location of the HII regions, we can speculate that these young star-forming regions are potential precursors of globular clusters that will be part of the halo of NGC 2865 in the future. Our result supports the use of the multi-slit imaging spectroscopy as a useful tool for finding nearly-formed stellar systems around galaxies.

Key words. ISM: abundances – HII regions – galaxies: dwarf – galaxies: ISM – galaxies: star formation

1. Introduction

Galaxies may experience interactions and mergers throughout their lifetimes. Tidal forces distort galaxy shapes leading to the formation of different structures and substructures. These include shells, rings, tails, and lead to the onset of star formation inside and outside galaxies (e.g. Toomre 1977; Mendes de Oliveira et al. 2004; Schiminovich et al. 2013; Ueda et al. 2014; Ordenes-Briceño et al. 2016) depending on the nature and evolutionary stage of the on-going tidal interaction. In particular, after a close encounter of two gas-rich systems of similar mass, the gas may be stripped from the interacting galaxies forming long filaments or tidal tails driven by gravity torques (e.g. the Antennae galaxies, which are the nearest example of merging disk galaxies in the Toomre 1977 sequence), while the stars mostly remain in the system, given their higher velocity dispersions and their collisionless dynamics. Once the gas has been removed, it can cool, self-gravitate and form new stars (Duc 2012). Thus, these systems are ideal laboratories to study star formation in extreme environments, in particular outside galaxies, in regions where, under normal conditions, the gas density would have been too low for star-formation to occur (Maybhate et al. 2007; Sengupta et al. 2015).

The details of the processes capable of triggering star formation in the low-density environments of galaxies outskirts and in the intergalactic medium are still not fully understood. Numerical simulations done to study the dynamics of interacting and merging galaxies (e.g. Bournaud et al. 2008, 2010; Escala et al. 2013; Renaud et al. 2015) have shown that young stellar substructures are formed in the outskirts of merger remnants as well as outside galaxies, in gas clouds stipped during interactions. These simulated objects have properties similar to the observed ones: the largest objects are usually formed at the tip of the tails and the objects have low mass-luminosity (M/L) ratios and high metallicities. Indeed the actively star-forming regions associated with the galaxy outskirts or intergalactic medium (e.g. Neff et al. 2004; Lisenfeld et al. 2007; Knierman et al. 2012; Mullan et al. 2013) have high metallicities for their luminosities, given that they are formed by gas that was pre-enriched in the "parent" galaxy (e.g. Mendes de Oliveira et al. 2004; Duc et al. 2007; de Mello et al. 2012; Torres-Flores et al. 2012, 2014). The evolution of the newly formed systems is mainly driven by

gravitational turbulence and instabilities around the Jeans-Scale (Bournaud et al. 2010).

Most of the studies on star-forming regions in the outskirts of galaxies are based in the analysis of ongoing wet mergers, where HI-rich tidal debris and tidal structures are present, and the interacting galaxies are still separate entities (e.g. Oosterloo et al. 2004; Mendes de Oliveira et al. 2004, 2006; Ryan-Weber et al. 2004; Boquien et al. 2007; Torres-Flores et al. 2012; de Mello et al. 2012; Rodruck et al. 2016; Lee-Waddell et al. 2016). However, the environments of peculiar merger-candidate elliptical galaxies, with HI outside their main optical body, have not receive as much attention. This is an interesting variation given that these systems are in advanced stages of evolution. Rampazzo et al. (2007) have shown a few examples of "rejuvenated" elliptical galaxies, which display young bursts of star formation. The object of study in this paper is one of these rejuvenated ellipticals. NGC 2865, a genuinely peculiar elliptical galaxy, with a surface brightness profile consistent with $r^{1/4}$, inside its effective radius (Jørgensen et al. 1992), but deep images show shells and disturbed morphology, present in merging systems (Rampazzo et al. 2007). NGC 2865, at a distance of 38 Mpc, has an extended tidal tail of HI gas, settled in a ring around the galaxy, with low surface brightness optical counterpart. The fine structures present around the galaxy are shells, very faint filaments and an outer loop, that are indicative of an advanced stage of interaction of ∼4 Gyr (Malin & Carter 1983; Hau et al. 1999).

In Urrutia-Viscarra et al. (2014, hereafter UV14) we obtained a complete census of Hα-emitting sources in the south-eastern region of the HI ring of NGC 2865 using the multi-slit imaging spectroscopy (MSIS) technique (Gerhard et al. 2005; Arnaboldi et al. 2007). Using this technique (a combination of a mask of parallel multiple slits with a narrow-band filter centered around the Hα line, see UV14 for details), seven candidate intergalactic HII regions were detected. Due to the short wavelength interval (∼80 Å) of the spectra, only one emission line (Hα) was typically detected. We were, then, not able to confirm the redshifts and compute the metallicities using just one line. Thus, here we revisited NGC 2865 using multi-object spectroscopy of five of the seven HII regions previously detected.We placed two slits over one of these regions, which were resolved into two different regions. The large wavelength interval used in the new observations, from 4500 Å to 7000 Å allowed us to confirm the nature of the sources as newly formed objects and to derive their main physical parameters.

The paper is organized as follows. In Sect. 2 we describe the observation and the data reduction. The analysis and results are described in Sect. 3. We discuss our results in Sect. 4 and present our conclusions in Sect. 5.

Throughout this paper we use $H_0 = 75$ km s^{-1} Mpc^{-1} which results in a distance for NGC 2865 of 38 Mpc. At this distance, $1' = 11$ kpc. The systemic velocity of NGC 2865 is 2627 km s^{-1}

2. Observation and reduction

2.1. Observation

The data were collected with the Gemini Multi-Object Spectrograph (Hook et al. 2004, hereafter GMOS) mounted on the Gemini South telescope in Chile in queue mode (Program ID. GS-2011A-Q-55). Given that we wanted to compare the results with those obtained with the MSIS technique, our field of view is the same as observed in UV14. We observed the southeastern HI tail of NGC 2865 ($\alpha(2000) = 9^h23^m37\overset{s}{.}13$, $\delta(2000) = -23°11^m54\overset{s}{.}34$) in the g' filter on February 1, 2011 (UT) to build the multi-slit mask.

The spectra were observed between April 13 and April 27 2013, under gray and photometric conditions, and with a seeing ranging between $0\overset{''}{.}8$ and $1''$. We centered the slits in 20 sources across the GMOS field of view, five of which were previously identified in UV14. For the region IG_04 we set two slits, one in the stellar cluster (or main source) and the other in the tail, as is defined by UV14 To avoid confusion, we re-defined the ID of the region IG_04 as IG_04_main and IG_04_tail according to where we set the slit (see Fig. 1). The spectra in the mask were observed using the R400 grating, $1''$ slits, 2×2-binning, and centered at 6550. A total of 12 exposures of 1150 s each were obtained. An offset of 50 Å toward the blue or the red was performed, between successive exposures, such that the central wavelength ranged from 6400 Å to 6650 Å, to avoid losing any important emission lines that could fall, by chance, in the gaps between CCDs. Spectroscopic flat fields and CuAr comparison lamps spectra were taken before and after each science exposure.

2.2. Data reduction

All spectra were reduced with the Gemini GMOS package version 1.8 inside IRAF[1] following the standard procedures for MOS observations. Science exposures, spectroscopic flats and CuAr comparison lamps were overscan/bias-subtracted and trimmed. The two-dimensional science spectra were flat fielded, wavelength calibrated, rectified (S-shape distortion corrected) and extracted to one-dimensional format. The cosmic rays were removed using the Laplacian Cosmic Ray Identification algorithm (van Dokkum 2001). The final spectra have a resolution of ∼7.0 Å (as measured from the sky lines 5577 Å and 6300 Å) and a dispersion of 1.36 Å pixel^{-1}, with a typical coverage in wavelength between ∼4500 Å and ∼7000 Å (see Fig. 2).

The science spectra were flux calibrated using the spectrum of the spectrophotometric standard star LTT 7379 observed during the night of April 11, 2011 UT, under different observing program and with the same instrument setup used for the science spectra. The standard star being observed in a different night ensures good relative flux calibration, although probably an uncertain absolute zero point. The flux standard was reduced following the same procedures used for the science frames.

2.3. Emission lines

The six spectra exhibit strong emission lines of Hα and [NII]λ6583 Å. Four of the six spectra also show Hβ and the forbidden lines: [OIII]$\lambda\lambda$4959, 5007 Å and [SII]$\lambda\lambda$6717, 6731 Å. No significant underlying continuum was measured in any of the six cases, hence no continuum subtraction was done. The principal parameters for each spectrum presented in Table 1 are: Col. (1): ID; Col. (2), the central wavelength for the Hα emission line; Col. (3), the heliocentric velocity, obtained with the task RVIDLINE from IRAF (using at least three emission lines); Col. (4), the projected distance (from the center of NGC 2865) in kpc; and Col. (5), line ratios Hα/Hβ. The latter was used to estimate the color excess, $E(B-V)$ (see Sect. 3.1). The errors for the velocities listed in Col. (3) were estimated using Monte Carlo

[1] IRAF is distributed by the National Optical Astronomy Observatories,which are operated by the Association of Universities of Research in Astronomy, Inc., under cooperative agreement with the NSF.

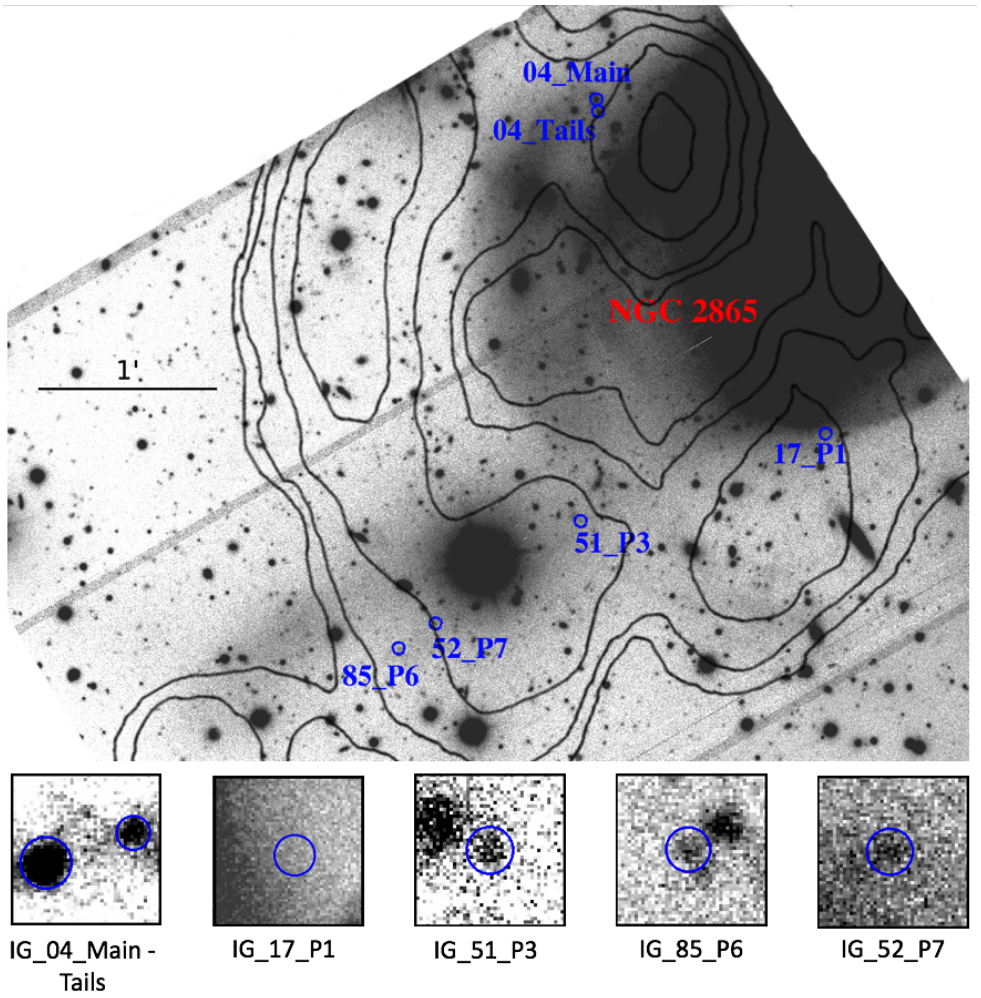

Fig. 1. Gemini g'-band images, the regions are marked and a zoom is show for each one. The size of the magnified images are 6.5″ × 6.5″. A radius of 1″ was used in the photometry, which are indicate in the magnified images. North is up and east is to the left.

Table 1. Physical properties of the intergalactic HII regions.

ID	λHα Å	V_{sys} km s^{-1}	$D_{projected}$ Kpc	Line ratio Hα/Hβ
IG_04_main	6618	2571	16	7.27
IG_04_tail	6616	2471	16	6.84
IG_17_P1	6617	2461	15	–
IG_51_P3	6615	2360	26	4.06
IG_85_P6	6614	2341	40	–
IG_52_P7	6614	2331	37	6.00

simulations for 100 runs, and were found to be ∼40 km s^{-1} for each spectrum.

3. Analysis and results

For each of the six regions, when possible, we derived the following parameters: i) color excess $E(B-V)$; ii) oxygen abundance, 12 + log(O/H); and iii) electron density, n_e. These results are used in the following analysis of the physical and chemical properties of the HII regions around NGC 2865.

3.1. Reddening correction E(B – V)

Dust extinction in each region was estimated from the line ratio Hα/Hβ (Calzetti et al. 1994). The intrinsic value for the Hα_0/Hβ_0 ratio for an effective temperature of 10^4 K and $N_e = 10^2$ cm^{-3} is 2.863 (Osterbrock & Ferland 2006). Thus, we estimated the extinction using the following relation (Osterbrock & Ferland 2006):

$$\frac{I_\lambda}{I_{H\beta}} = \frac{I_{\lambda 0}}{I_{H\beta 0}} 10^{-c[f(\lambda)-f(H\beta)]} \quad (1)$$

where I_λ and $I_{\lambda 0}$ are the observed and the theoretical fluxes, respectively. c is the reddening coefficient and $f(\lambda)$ is the reddening curve. The line ratios Hα/Hβ used to estimate the dust extinction values are tabulated in Table 1.

The relation between $E(B-V)$ and c depends on the shape of the extinction curve; assuming a Galactic standard extinction curve ($R = 3.1$, typical in the diffuse interstellar medium) and the Hα line ($\lambda = 6563$ Å), the values for each parameter are: $f(H\beta) = 1.164$, $f(H\alpha) = 0.818$. Thus, the color excess is given by $E(B-V) \approx 0.77c$.

For the spectra IG_04_main, IG_04_tail, IG_51_P3 and IG_52_P7 the color excess was obtained using the Hα and Hβ lines, as described above. Given that Hβ emission is not detected in the spectra of IG_17_P1 and IG_85_P6, we used in these cases a correction equal to the average of the color excess

Table 2. Line intensities of the Intergalactic HII regions around NGC 2865.

ID	Flux$_{H\beta}$	Flux$_{[OIII]\lambda5007}$	Flux$_{H\alpha}$	Flux$_{[NII]\lambda6583}$	Flux$_{[SII]\lambda6717}$	Flux$_{[SII]\lambda6731}$
IG_04_main	0.49 ± 0.06	1.12 ± 0.36	1.27 ± 0.67	0.52 ± 0.16	0.22 ± 0.03	0.20 ± 0.07
IG_04_tail	2.41 ± 0.97	7.00 ± 0.76	7.63 ± 1.23	2.15 ± 0.36	1.16 ± 0.35	0.69 ± 0.23
IG_17_P1	–	0.12 ± 0.05	0.13 ± 0.02	0.03 ± 0.01	–	–
IG_51_P3	0.04 ± 0.01	–	0.18 ± 0.05	0.05 ± 0.01	–	–
IG_85_P6	–	–	0.55 ± 0.13	0.15 ± 0.03	0.09 ± 0.06	0.07 ± 0.09
IG_52_P7	0.16 ± 0.35	0.10 ± 0.74	0.29 ± 0.46	0.08 ± 0.02	0.06 ± 0.01	0.04 ± 0.02

Notes. The fluxes are in units of 10^{-15} erg s^{-1} cm^{-2}.

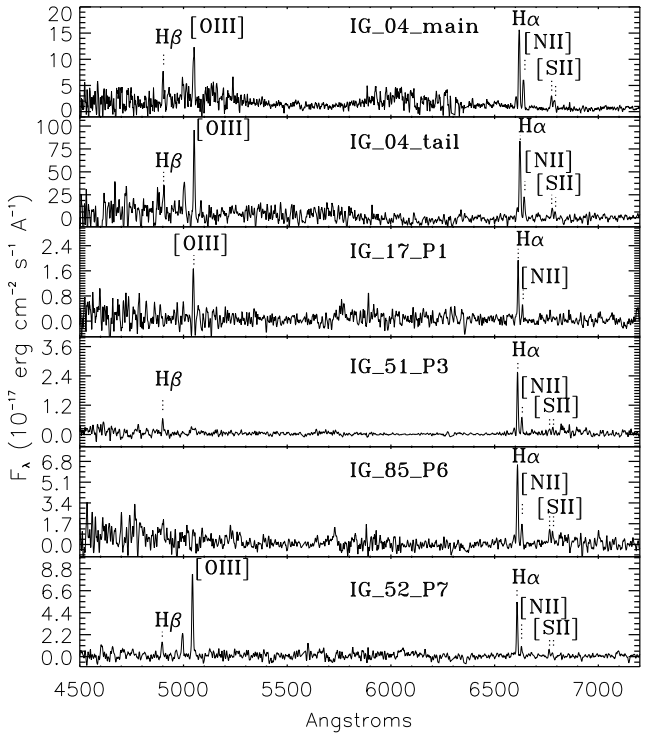

Fig. 2. Spectra for six intergalactic regions around NGC 2865. Including IG_04_tail.

obtained in the other four regions. We corrected each spectrum for the interstellar dust extinction using the extinction function given by Calzetti et al. (2000). This is thought to be appropriate for de-reddening the spectrum of a source whose output radiation is dominated by massive stars, as we assume the regions observed here are.

The six extracted spectra after the extinction correction are shown in Fig. 2. The lines used are marked in each spectrum. In Table 2 we list the resulting fluxes, after the reddening correction is applied.

The four HII regions for which it was possible to estimate the reddening correction, present high values of color excess, $E(B-V) > 0.33$. These values indicate a considerably high dust absorption, typical of a nebula where newborn stars are being formed (Arias et al. 2006). Indeed, these four regions display quite young ages, as derived by UV14, ranging from ~2 to 50 Myr, which strongly suggests that these sources are the birthplace of young stars.

3.2. Oxygen abundance

The most commonly measured tracers of metallicity are oxygen and iron, given their bright spectral lines. Iron is usually used as a metallicity indicator when old stars are the main component, while oxygen is the metallicity tracer of choice in the interstellar medium (Henry & Worthey 1999).

In the ionized gas the most accurate estimator to derive the chemical abundance is the electron temperature, T_e (Osterbrock & Ferland 2006). In the optical, T_e can be estimated using sensitive lines such as [OIIIλ4363 Å]. However, the auroral lines are difficult to detect in extragalactic star forming regions, where cooling is efficient and the temperature is low. Thus, strong nebular lines must be used to derive oxygen abundances (e.g. Denicoló et al. 2002; Pilyugin 2001; Pettini & Pagel 2004). The empirical methods more frequently use the N_2 and O_3N_2 indices,

$$N_2 \equiv \log\left(\frac{I([\mathrm{NII}]\lambda6583)}{I(\mathrm{H}\alpha)}\right) \quad (2)$$

$$O_3N_2 \equiv \log\left(\frac{I([\mathrm{OIII}]\lambda5007)}{I(\mathrm{H}\beta)}\Big/\frac{I([\mathrm{NII}]\lambda6583)}{I(\mathrm{H}\alpha)}\right). \quad (3)$$

We calculated the oxygen abundances using the empirical methods N_2 and, when possible, also O_3N_2, as proposed and calibrated by Pettini & Pagel (2004). These "empirical" methods are adequate for estimating oxygen abundances in extragalactic HII regions. We used the linear relation between the oxygen abundance and the N_2 index given by:

$$12 + \log(\mathrm{O/H}) = 8.90 + 0.57 \times N_2 \quad (4)$$

Three regions have the four lines; for these we were able to use the index O_3N_2 and the linear relation between the O_3N_2 and the oxygen abundance given by:

$$12 + \log(\mathrm{O/H}) = 8.73 - 0.32 \times O_3N_2. \quad (5)$$

The uncertainties in the calibration of these methods are 0.18 dex and 0.14 dex (at the 68% confidence interval), for N_2 and O_3N_2, respectively. Table 3 lists the oxygen abundances estimated including the values of the N_2 and O_3N_2 indices for each region.

In Table 3 we summarize the oxygen abundances calculated for all of our HII regions. using the N_2 index. We found an excellent agreement between the values derived from the N_2 and the O_3N_2 indices. The average value for the oxygen abundance for the six regions is $12 + \log(\mathrm{O/H}) \sim 8.6$, which is very similar to typical values for extragalactic HII regions reported in the literature for other interacting systems (e.g. Werk et al. 2010; Torres-Flores et al. 2012; de Mello et al. 2012; Olave-Rojas et al. 2015).

3.3. Electron density

The electron density, N_e, is one of the fundamental physical parameters used to characterize HII regions. It is a reliable

Table 3. Physical parameters derived from spectral lines for the intergalactic HII regions.

ID	$M_{g'}$ mag	N_e cm^{-3}	$E(B-V)$	N_2	O_3N_2	12+log(O/H) N_2	12+log(O/H) O_3N_2
IG_04_main	–15.76	327	0.91	–0.39	0.74	8.67 ± 0.18	8.49 ± 0.1
IG_04_tail	–15.31	90	0.84	–0.54	1.01	8.58 ± 0.18	8.40 ± 0.14
IG_17_P1	–	–	0.70*	–0.58	–	8.56 ± 0.18	–
IG_51_P3	–14.58	–	0.33	–0.54	–	8.58 ± 0.18	–
IG_85_P6	–14.22	176	0.70*	–0.54	—	8.58 ± 0.18	–
IG_52_P7	–14.51	176	0.75	–0.65	1.29	8.52 ± 0.18	8.31 ± 0.14

Notes. (*) Given that the Hβ emission line was not detected in two cases, the color excess, $E(B-V)$, was assumed to be an average of the values derived for the other four spectra.

physical quantity that is not sensitive to flux calibration errors and reddening. It is largely independent of metallicity, and only weakly depends on electron temperature. The most used emission lines to measure N_e are [OII]λ3729 Å/λ3726 Å, and [SII]λ6716 Å/λ6731 Å. Given the wavelength range of our spectra, N_e was determined for four HII regions based on the measured intensity ratio [SII]λ6716 Å/λ6731 Å. We used the task TEMDEN, available in the NEBULAR package of STSDAS, inside IRAF V2.16. For the calculation we assume an electron temperature of 10^4 K, which is a representative value for HII regions (Osterbrock & Ferland 2006). This assumption was necessary, given that we have no independent measurements for the temperatures of these regions.

It was possible to obtain the electron density for four of the six HII regions, see Table 3. We estimated values which ranged from 90 to 327 cm^{-3}, which are typical values of the electron density observed in the Magallanic Clouds (Feast 1964), and in particular for bright regions in 30 Dorado (Osterbrock & Ferland 2006).

In Table 3 we list the physical parameters described above using the [OIII], Hβ, [NII], Hα and [SII] lines of the intergalactic HII regions. All parameters were obtained after applying reddening correction.

3.4. Confirming the MSIS technique as an effective tool to find emission-line regions

The MSIS technique has been successfully used to detect extragalactic planetary nebulae in the Coma and Hydra I clusters (e.g. Gerhard et al. 2005; Ventimiglia et al. 2011). This technique combines a mask of parallel multiple slits with a narrow-band filter, centered around the [OIII] λ5007 Å line, at the redshift of the object. In the case of the Coma cluster, Gerhard et al. (2005) were able to detect faint objects with fluxes as low as 10^{-18} erg s^{-1} cm^{-2} Å^{-1}. An attempt to use the same technique to detect star-forming regions in the outskirts of galaxies was done by UV14, for the case of NGC 2865. Given the higher contrast between emission and background, this technique has great potential to detect faint emission-line objects when regular narrow-band imaging would fail to lead to a detection of faint objects. However, given that the spectral range observed with such a technique is limited, the spectra shown in this paper were a necessary follow-up to validate the efficiency of the MSIS method.

In the present paper we find that all of the detected objects with MSIS technique (UV14) for which further spectroscopic follow-up was done, were confirmed to be star-forming regions. This demonstrates that the MSIS technique is very efficient in finding emission-line objects.

This type of technique will become increasingly useful as the new generation of extremely large telescopes comes on-line and blind searches for emission-line objects can be done efficiently.

4. Discussion

In the previous sections, we described the main properties of the six intergalactic HII regions found in the southeast ring of HI gas within a radius of ~50 kpc of the elliptical galaxy NGC 2865. The study is based on 6 emission lines: Hβ, [OIII]λ 5007 Å, Hα, [NII], and SII$\lambda\lambda$ 6717, 6731 Å. The six regions were previously detected using the MSIS technique by UV14, but only one line (Hα) was observed then. The detection of at least three emission lines in each of the six regions, shown in this work, indicate that the sources have a velocity difference of ~50–300 km s^{-1} with respect to the systemic velocity of NGC 2865 and they have close to solar oxygen abundance (12 + log (O/H) ≈ 8.6, Asplund et al. 2009).

4.1. Star formation outside galaxies

The six intergalactic HII regions are located 16–40 kpc from the center of NGC 2865 and they show strong emission in Hα and low or absent continuum. The indication that they are young come from the ages derived in UV14, from ultraviolet fluxes, but our new observations constrain the ages further: high emission in Hα is a direct indicator of recent star formation, showing that the most recent starburst occurred less than 10 Myr ago, assuming single stellar populations (Leitherer et al. 1999).

Indication that they are formed in situ come from the prohibitively large velocities derived for these regions under the assumption that they traveled from inside the parent galaxy to the present location. Approximate velocities can be derived in back-of-envelope calculations, taking as an input the projected distance of the objects (with respect to the parent galaxy) and the derived ages. If the intergalactic HII regions were thrown out of the disk of the main galaxy during an interaction, the typical velocities they would need to have is over 16 kpc/10 Myr ≈ 1600 km s^{-1}. Such velocity is not expected, given the low velocity dispersions present in the field or in groups of galaxies (typically 200 km s^{-1}), arguing in favor of in-situ formation.

In addition, their metallicities were found to be close to solar. These high metallicities could be explained if the regions were formed out of enriched gas which was removed from the galaxy during the merger event. Thus, these regions are similar to extragalactic HII regions found in recent or ongoing mergers (e.g. Mendes de Oliveira et al. 2001; de Mello et al. 2012; Olave-Rojas et al. 2015). Torres-Flores et al. (2012) found

similar objects around the system NGC 2782, an ongoing merging galaxy which shows optical and HI tidal tails containing several HII regions. These objects have ages of between 1 and 11 Myr, masses ranging from 0.8−4 × 10^4 $M_\odot$ and solar metallicities, similar properties to those of the regions found in the present work.

Other examples of star formation outside galaxies is provided by the intra-cluster compact HII regions detected in the Virgo core, close to NGC 4388 (Gerhard et al. 2002). These objects have ages of about 3 Myr, mass of the order of 4 × 10^2 $M_\odot$ and metallicity 0.25 solar.

What makes NGC 2865 a special target for searches of newly-formed star forming objects is its evolutionary stage. This galaxy is a merger relic, an elliptical galaxy with an $r^{1/4}$ profile and low surface brightness tidal tails. Its last major merger happened ∼4 Gyr ago (Schiminovich et al. 1995). Nevertheless, NGC 2865, in such an advanced stage of evolution, proved to contain star forming regions with very similar properties to those found in less evolved systems.

4.2. The faint-continuum sources in low N_{HI} regions

The regions measured in this work have weak emission in the far- and near- ultraviolet (∼log(FUV) ∼ 37, ∼log(NUV) ∼ 36 erg s^{-1} $Å^{-1}$) and mass of Log($M_\star$) ∼ 6 $M_\odot$. Five of the six regions have low fluxes in the g'-band, $M_{g'} > 15.76$ and one of them is not seen at all in the Gemini/GMOS images (i.e. which sets a lower limit of 21 mag in g' for the magnitude of the object). Regions with such faint optical counterparts can only be found in blind searches such as those done using the MSIS technique.

Maybhate et al. (2007) and Mullan et al. (2013) reported that the threshold N_{HI} value to form stars in tidal debris of interacting galaxies is log(N_{HI}) ≈ 20.6 cm^{-2}, which is considered a necessary but not a sufficient condition to generate clusters. In the case of NGC 2865, this value is one order of magnitude lower with HI density of ∼3.8 × 10^{19} cm^{-2}, although it is possible that the real HI column densities are underestimated due to the large size of the beam (Schiminovich et al. 1995). The level of star formation in the southeast HI cloud where the regions of NGC 2865 are located is 2.6 × 10^{-3} $M_\odot$ yr^{-1} (UV14), that is similar to values observed in other systems such as in the Leo ring and in NGC 4262 (Thilker et al. 2009; Bettoni et al. 2010).

The mechanisms that trigger and quench star formation in such low-gas density environments is still a mistery. However, we can say that star formation does happen outside galaxies, in low HI column density regions, in different systems, including around at least one merger relic, NGC 2865.

4.3. Are HI tidal debris and tails nurseries of future globular clusters?

NGC 2865 is a shell galaxy (Malin & Carter 1983) with a peculiar morphology, embedded in a ring-shape HI tidal tail (see Fig. 1 and also Schiminovich et al. 1995). These features all point to a formation scenario for the galaxy as a wet merger. Using stellar spectroscopy and *UBV* images, Schiminovich et al. (1995) proposed that a possible major merger event happened between 1 and 4 Gyr ago. Rampazzo et al. (2007) found a young stellar sub-population in this galaxy with an age of 1.8 ± 0.5 Gyr. This finding is in agreement with the results obtained by Hau et al. (1999), who derived burst ages from population synthesis of 0.4−1.7 Gyr, indicating the presence of a younger stellar population in the core of NGC 2865. These authors also derived a much younger age for the shells of this galaxy. Salinas et al. (2015) and Sikkema et al. (2006) found a very blue population of globular clusters (GCs) with a color distribution which peaked at $(V - I) = 0.7$. This suggests the presence of stellar populations with ages ranging from 0.5 to 1 Gyr, similar to those found by Hau et al. (1999) in the central regions of NGC 2865. Moreover, Trancho et al. (2014) found a sub-population of young metal-rich GCs of age ∼1.8 ± 0.8 Gyr.

In this paper we have found a much younger sub-population, formed by emission-line regions, with an age <10 Myr (as indicated by the Hα-line emission). All these young regions are located in the HI tidal tails and they could be the result of a more recent burst of star formation. In UV14, we estimated a mass for these regions between 4 × 10^4 and 5 × 10^6 $M_\odot$. Similar values were found by Maraston et al. (2004) for the mass of a young cluster in the merger remnant NGC 7252 and by Goudfrooij et al. (2001) for the masses of clusters around the peculiar central galaxy of the Fornax cluster, NGC 1316, which is also considered a merger remnant.

In conclusion, NGC 2865 contains at least three generations of star clusters, the youngest generation (which is embedded in its HII regions) is the object of study of this paper. We do not exclude the possibility that these young HII regions could be the progenitors of the intermediate age or the red globular clusters that will be part of the halo of the future relaxed elliptical galaxy.

5. Conclusions

We have confirmed the tidal origin of six HII regions in the immediate vicinity of NGC 2865, previously detected using the MSIS technique. Our results show that although NGC 2865 has undergone a major merger event ∼4 Gyr ago, stars are still being formed in its HI tidal tail, outside the main body of the galaxy.

The HII regions around NGC 2865 display high oxygen abundances of 12 + log(O/H) ∼ 8.6. This suggests that they were formed from pre-processed and enriched material from the parent galaxy which was stripped to the intergalactic medium during a merger event. The objects coincide with a gaseous tail with a projected HI density of $N_{HI} < 10^{19}$ cm^{-2}, which is one magnitude lower than the HI critical density for star formation, as given by previous studies. The young regions (<10 Myr) found in this work can be associated with the youngest population in addition to the two populations of star clusters already identified in NGC 2865: i) a much older generation of globular clusters; and ii) a secondary population with an age ranging from 0.5 to 1.8 Gyr, as found by Sikkema et al. (2006) and Trancho et al. (2014).

The fate of these young sources is unclear: they may either get re-acreted onto the parent galaxy, get dissolved or merge to form massive (globular) star clusters. Indeed, given the mass and the location of the HII regions, we can not exclude that these young star-forming regions are potential precursors of globular clusters that will be part of the halo of NGC 2865. The latter scenario is consistent with the results obtained by Bournaud et al. (2008), who used high-resolution simulations of galaxies mergers. These authors found that super star cluster formed in mergers are likely the progenitors of globular clusters. In this sense, our observations are in agreement with the predictions derived from simulations.

Finally, in this paper we verify that the MSIS technique is a powerful tool to detect faint objects with emission lines which are not always detected in broad band imaging. This technique may become specially useful in blind searches of emission line

objects to be done with the next generation of extremely large telescopes.

Acknowledgements. The authors would like to thank the anonymous referee for the thoughtful comments which improved the clarity of this paper. Based on observations obtained at the Gemini Observatory, which is operated by the Association of Universities for Research in Astronomy, Inc., under a cooperative agreement with the NSF on behalf of the Gemini partnership: the National Science Foundation (United States), the National Research Council (Canada), CONICYT (Chile), Ministerio de Ciencia, Tecnología e Innovación Productiva (Argentina), and Ministério da Ciência, Tecnologia e Inovação (Brazil). F.U.-V. acknowledges the financial support of the Chilean agency Conicyt + PAI/Concurso nacional apoyo al retorno de investigadores/as desde el extranjero, convocatoria 2014, under de contract 82140065. S.T.-F. acknowledges the financial support of Dirección de Investigación y Desarrollo de la ULS, through a project DIULS Regular, under contract PR16143. C.M.d.O. acknowledges support from FAPESP (grants 2009/54202-8, 2016/17119-9) and CNPq (grant 312333/2014-5). S.T.-F. and C.M.d.O. acknowledge financial support of CONICYT + PAI/Atracción de Capital Humano Avanzado del Extranjero, Folio N PAI80160082.

References

Arias, J. I., Barbá, R. H., Maíz Apellániz, J., Morrell, N. I., & Rubio, M. 2006, MNRAS, 366, 739
Arnaboldi, M., Gerhard, O., Okamura, S., et al. 2007, PASJ, 59, 419
Arp, H. 1966, ApJS, 14, 1
Asplund, M., Grevesse, N., Sauval, A. J., & Scott, P. 2009, ARA&A, 47, 481
Bettoni, D., Buson, L. M., & Galletta, G. 2010, A&A, 519, A72
Boquien, M., Duc, P.-A., Braine, J., et al. 2007, A&A, 467, 93
Bournaud, F., Duc, P.-A., & Emsellem, E. 2008, MNRAS, 389, L8
Bournaud, F., Elmegreen, B. G., Teyssier, R., Block, D. L., & Puerari, I. 2010, MNRAS, 409, 1088
Calzetti, D., Kinney, A. L., & Storchi-Bergmann, T. 1994, ApJ, 429, 582
Calzetti, D., Armus, L., Bohlin, R. C., et al. 2000, ApJ, 533, 682
de Mello, D. F., Urrutia-Viscarra, F., Mendes de Oliveira, C., et al. 2012, MNRAS, 426, 2441
Denicoló, G., Terlevich, R., & Terlevich, E. 2002, MNRAS, 330, 69
Duc, P.-A. 2012, in Dwarf Galaxies: Keys to Galaxy Formation and Evolution, Astrophys. Space Sci. Proc., 28, 305
Duc, P.-A., Braine, J., Lisenfeld, U., Brinks, E., & Boquien, M. 2007, A&A, 475, 187
Escala, A., Becerra, F., del Valle, L., & Castillo, E. 2013, ApJ, 763, 39
Fall, S. M., Chandar, R., & Whitmore, B. C. 2005, ApJ, 631, L133
Feast, M. W. 1964, MNRAS, 128, 327
Gerhard, O., Arnaboldi, M., Freeman, K. C., & Okamura, S. 2002, ApJ, 580, L121
Gerhard, O., Arnaboldi, M., Freeman, K. C., et al. 2005, ApJ, 621, L93
Goudfrooij, P., Mack, J., Kissler-Patig, M., Meylan, G., & Minniti, D. 2001, MNRAS, 322, 643
Hau, G. K. T., Carter, D., & Balcells, M. 1999, MNRAS, 306, 437
Henry, R. B. C., & Worthey, G. 1999, PASP, 111, 919
Hernquist, L., & Spergel, D. N. 1992, ApJ, 399, L117
Hibbard, J. E., & van Gorkom, J. H. 1996, AJ, 111, 655
Hibbard, J. E., van Gorkom, J. H., Rupen, M. P., & Schiminovich, D. 2001, ASP Conf. Ser., 240, 657
Hook, I. M., Jørgensen, I., Allington-Smith, J. R., et al. 2004, PASP, 116, 425
Horellou, C., & Koribalski, B. S. 2004, IAU Symp., 217, 422
Jorgensen, I., Franx, M., & Kjaergaard, P. 1992, A&AS, 95, 489
Knierman, K., Knezek, P. M., Scowen, P., Jansen, R. A., & Wehner, E. 2012, ApJ, 749, L1
Lada, C. J., & Lada, E. A. 2003, ARA&A, 41, 57
Lee-Waddell, K., Spekkens, K., Chandra, & P., et al. 2016, MNRAS, 460, 2945
Leitherer, C., Schaerer, D., Goldader, J. D., et al. 1999, ApJS, 123, 3
Lisenfeld, U., Mundell, C., Allsopp, J., & Schinnerer, E. 2007, New Astron., 51, 63
Malin, D. F., & Carter, D. 1980, Nature, 285, 643
Malin, D. F., & Carter, D. 1983, ApJ, 274, 534
Maraston, C., Bastian, N., Saglia, R. P., et al. 2004, A&A, 416, 467
Maybhate, A., Masiero, J., Hibbard, J. E., et al. 2007, MNRAS, 381, 59
Mendes de Oliveira, C., Plana, H., Amram, P., Balkowski, C., & Bolte, M. 2001, AJ, 121, 2524
Mendes de Oliveira, C., Cypriano, E. S., Sodré, L., Jr., & Balkowski, C. 2004, ApJ, 605, L17
Mendes de Oliveira, C. L., Temporin, S., Cypriano, E. S., et al. 2006, AJ, 132, 570
Mullan, B., Kepley, A. A., Maybhate, A., et al. 2013, ApJ, 768, 194
Neff, S. G., Thilker, D., Hibbard, J. E., et al. 2004, Am. Astron. Soc. Meeting, 2005, 25.05
Olave-Rojas, D., Torres-Flores, S., Carrasco, E. R., et al. 2015, MNRAS, 453, 2808
Ordenes-Briceño, Y., Georgiev, I. Y., Puzia, T. H., Goudfrooij, P., & Arnaboldi, M. 2016, A&A, 585, A156
Osterbrock, D. E., & Ferland, G. J. 2006, Astrophysics of gaseous nebulae and active galactic nuclei (CA: University Science Books)
Oosterloo, T., Morganti, R., Sadler, E. M., et al. 2004, IAU Symp., 217, 486
Pettini, M., & Pagel, B. E. J. 2004, MNRAS, 348, L59
Pilyugin, L. S. 2001, A&A, 369, 594
Rampazzo, R., Marino, A., Tantalo, R., et al. 2007, MNRAS, 381, 245
Renaud, F., Bournaud, F., & Duc, P.-A. 2015, MNRAS, 446, 2038
Rodruck, M., Konstantopoulos, I., Knierman, K., et al. 2016, MNRAS, 461, 36
Ryan-Weber, E. V., Meurer, G. R., Freeman, K. C., et al. 2004, AJ, 127, 1431
Salinas, R., Alabi, A., Richtler, T., & Lane, R. R. 2015, A&A, 577, A59
Schiminovich, D., van Gorkom, J. H., van der Hulst, J. M., & Malin, D. F. 1995, ApJ, 444, L77
Schiminovich, D., van Gorkom, J. H., & van der Hulst, J. M. 2013, AJ, 145, 34
Schweizer, F., Burns, C. R., Madore, B. F., et al. 2008, AJ, 136, 1482
Sengupta, C., Scott, T. C., Paudel, S., et al. 2015, A&A, 584, A114
Serra, P., Oosterloo, T., Morganti, R., et al. 2012, MNRAS, 422, 1835
Sikkema, G., Peletier, R. F., Carter, D., Valentijn, E. A., & Balcells, M. 2006, A&A, 458, 53
Stahler, S. W., & Palla, F. 2005, The Formation of Stars (Wiley-VCH)
Thilker, D. A., Donovan, J., Schiminovich, D., et al. 2009, Nature, 457, 990
Toomre, A. 1977, in The New Astronomy and Space Science Reader (San Francisco, CA: W.H. Freeman and Company), 401
Toomre, A., & Toomre, J. 1972, ApJ, 178, 623
Torres-Flores, S., de Oliveira, C. M., de Mello, D. F., Scarano, S., & Urrutia-Viscarra, F. 2012, MNRAS, 421, 3612
Torres-Flores, S., Scarano, S., Mendes de Oliveira, C., et al. 2014, MNRAS, 438, 1894
Trancho, G., Miller, B. W., Schweizer, F., Burdett, D. P., & Palamara, D. 2014, ApJ, 790, 122
Ueda, J., Iono, D., Yun, M. S., et al. 2014, ApJS, 214, 1
Urrutia-Viscarra, F., Arnaboldi, M., Mendes de Oliveira, C., et al. 2014, A&A, 569, A97
Werk, J. K., Putman, M. E., Meurer, G. R., et al. 2010, ApJ, 715, 656
van Dokkum, P. G. 2001, PASP, 113, 1420
Ventimiglia, G., Arnaboldi, M., & Gerhard, O. 2011, A&A, 528, A24
Zwicky, F. 1956, Irish Astron. J., 4, 61